ELectronics EXpress

LETTER

IEICE Electronics Express, Vol.13, No.22, 1–12

The distribution of electromagnetic waves and forces in a dispersive chiral cylinder

Guiping Li, Maoyan Wang[a)], Hailong Li, Mengxia Yu, Xiaochuan Zhang, Zhitao Xu, and Jun Xu

School of Physical Electronics, University of Electronic Science and Technology of China, No. 4, Section 2, North Jianshe Road, Cheng du, P. R. China

a) *wmybrimlhl@uestc.edu.cn*

Abstract: By introducing the effects of bound electric and magnetic charges, the mechanical interaction between waves and a chiral cylinder is investigated with the auxiliary differential equations finite-difference time-domain method. The trapping Lorentz force density distributions of an active chiral cylinder, as well as a core-shell cylinder consisting of a chiral shell and a dielectric core illuminated by a normally incident plane wave are simulated. Numerical results show that the working principle is based on gradient forces generated by the continuously coupled cross-polarized waves. This finding may provide a promising avenue in chirality detection and sorting chiral particles from achiral ones.

Keywords: chiral media, electromagnetic, optics, dispersion

Classification: Optical systems

References

[1] A. Ashkin, *et al.*: "Observation of a single-beam gradient force optical trap for dielectric particles," Opt. Lett. **11** (1986) 288 (DOI: 10.1364/OL.11.000288).

[2] D. Gao, *et al.*: "Macroscopic broadband optical escalator with force-loaded transformation optics," Opt. Express **21** (2013) 796 (DOI: 10.1364/OE.21.000796).

[3] A. Akbarzadeh, *et al.*: "Tracing optical force fields within graded-index media," New J. Phys. **16** (2014) 053035 (DOI: 10.1088/1367-2630/16/5/053035).

[4] A. Novitsky and C.-W. Qiu: "Pulling extremely anisotropic lossy particles using light without intensity gradient," Phys. Rev. A **90** (2014) 053815 (DOI: 10.1103/PhysRevA.90.053815).

[5] Q. C. Shang, *et al.*: "Analysis of the radiation force and torque exerted on a chiral sphere by a Gaussian beam," Opt. Express **21** (2013) 8677 (DOI: 10.1364/OE.21.008677).

[6] K. Ding, *et al.*: "Realization of optical pulling forces using chirality," Phys. Rev. A **89** (2014) 063825 (DOI: 10.1103/PhysRevA.89.063825).

[7] A. Canaguier-Durand, *et al.*: "Mechanical separation of chiral dipoles by chiral light," New J. Phys. **15** (2013) 123037 (DOI: 10.1088/1367-2630/15/12/123037).

DOI: 10.1587/elex.13.20160974
Received October 5, 2016
Accepted October 24, 2016
Publicized November 9, 2016
Copyedited November 25, 2016

[8] G. Tkachenko and E. Brasselet: "Helicity-dependent three-dimensional optical trapping of chiral microparticles," Nat. Commun. **5** (2014) 4491 (DOI: 10.1038/ncomms5491).
[9] K. J. Webb and Shivanand: "Negative electromagnetic plane-wave force in gain media," Phys. Rev. E **84** (2011) 057602 (DOI: 10.1103/PhysRevE.84.057602).
[10] A. Mizrahi and Y. Fainman: "Negative radiation pressure on gain medium structures," Opt. Express **35** (2010) 3405 (DOI: 10.1364/OL.35.003405).
[11] A. R. Zakharian, *et al.*: "Radiation pressure and the distribution of electromagnetic force in dielectric media," Opt. Express **13** (2005) 2321 (DOI: 10.1364/OPEX.13.002321).
[12] B. A. Kemp, *et al.*: "Ab initio study of the radiation pressure on dielectric and magnetic media," Opt. Express **13** (2005) 9280 (DOI: 10.1364/OPEX.13.009280).
[13] T. Kawasaki, *et al.*: "Self-replication and amplification of enantiomeric excess of chiral multifunctionalized large molecules by asymmetric autocatalysis," Angew. Chem. Int. Ed. **126** (2014) 11381 (DOI: 10.1002/ange.201405441).
[14] V. V. Pokropivny: "Non carbon nanotubes, synthesis, structure, properties and promising applications," Proc. 2001 Int. Conf. Hydrogen Materials Science and Chemistry of Metal Hydrides (2001) 630 (DOI: 10.1023/A:1015232003933).
[15] A. D. Falco: "Chiral plasmonic nanostructures: twisted by DNA," Nat. Mater. **13** (2014) 846 (DOI: 10.1038/nmat4068).
[16] M. Tateiba: "Theoretical study on wave propagation and scattering in random media and its application," IEICE Trans. Electron. **E93.C** (2010) 3 (DOI: 10.1587/transele.E93.C.3).
[17] G. P. Li, *et al.*: "Wave propagation and Lorentz force density in gain chiral structures," Opt. Mater. Express **6** (2016) 388 (DOI: 10.1364/OME.6.000388).
[18] B. N. Wang, *et al.*: "Chiral metamaterials: simulations and experiments," J. Opt. A, Pure Appl. Opt. **11** (2009) 114003 (DOI: 10.1088/1464-4258/11/11/114003).
[19] A. N. Nguyen and H. Shirai: "Electromagnetic scattering analysis from rectangular dielectric cuboids-TE polarization," IEICE Trans. Electron. **E99.C** (2016) 11 (DOI: 10.1587/transele.E99.C.11).
[20] K. Hannam, *et al.*: "Broadband chiral metamaterials with large optical activity," Phys. Rev. B **89** (2014) 125105 (DOI: 10.1103/PhysRevB.89.125105).
[21] S. G. Zhou, *et al.*: "Preliminary study on active modulation of polar mesosphere summer echoes with the radio propagation in layered space dusty plasma," Plasma Sci. Technol. **18** (2016) 607 (DOI: 10.1088/1009-0630/18/6/05).
[22] Z. Bertalan, *et al.*: "Navigation strategies of motor proteins on decorated tracks," PLoS One **10** (2015) e0136945 (DOI: 10.1371/journal.pone.0136945).
[23] S. Tretyakov, *et al.*: "Waves and energy in chiral nihility," J. Electromagn. Waves Appl. **17** (2003) 695 (DOI: 10.1163/156939303322226356).
[24] A. Taflove and S. C. Hagness: *Computational Electrodynamics: The Finite Difference Time–Domain Method* (Artech House, Norwood, MA, 2005) 3rd ed.
[25] K. S. Zheng, *et al.*: "Analysis of Doppler effect of moving conducting surfaces with Lorentz-FDTD method," J. Electromagn. Waves Appl. **27** (2013) 149 (DOI: 10.1080/09205071.2013.741042).
[26] M. Y. Wang, *et al.*: "The effect of media parameters on wave propagation in a chiral metamaterials slab using FDTD," Int. J. Numer. Model. **27** (2014) 109 (DOI: 10.1002/jnm.1902).
[27] Y. Zhao, *et al.*: "Accurate modeling of the optical properties of left-handed media using a finite-difference time-domain method," Phys. Rev. E **75** (2007) 037602 (DOI: 10.1103/PhysRevE.75.037602).

DOI: 10.1587/elex.13.20160974
Received October 5, 2016
Accepted October 24, 2016
Publicized November 9, 2016
Copyedited November 25, 2016

[28] J. A. Pereda, *et al.*: "FDTD modeling of chiral media by using the mobius transformation technique," IEEE Antennas Wireless Propag. Lett. **5** (2006) 327 (DOI: 10.1109/LAWP.2006.878902).
[29] I. V. Lindell, *et al.*: *Electromagnetic Waves in Chiral and Bi-isotropic Media* (Artech House, Boston, 1994).
[30] V. Demir, *et al.*: "FDTD formulation for dispersive chiral media using the Z transform method," IEEE Trans. Antennas Propag. **53** (2005) 3374 (DOI: 10.1109/TAP.2005.856328).
[31] M. Mansuripur: "On the foundational equations of the classical theory of electrodynamics," Resonance **18** (2013) 130 (DOI: 10.1007/s12045-013-0016-4).

1 Introduction

In recent years, optical forces [1, 2, 3, 4, 5, 6, 7, 8, 9, 10, 11, 12] in different structures and devices have been a subject of great interest because of theirs application in optical tweezers [2, 3, 4], tractor beams [5], etc. Most of these studies have been focused on the structures composed of passive materials [3, 4], whereas forces on active media have received little attention. Gain media with a positive imaginary part of the complex permittivity are simulated in Refs. [9, 10]. Active media [13, 14] may be modeled by chiral media with a large imaginary part of chirality parameter [5, 6, 7, 8]. The chirality parameter may reverse the sign of the optical forces. It has been demonstrated that chiral objects [7] can be mechanically separated based on their enantiomeric form by using the chiral light. It has also been shown that pulling forces can be realized via the coupling of the linear momentum of a chiral particle with the spin angular momentum of light [1].

Though the theory, experiments, and applications in particle-light interaction have been well established, there are some unknowns yet to be investigated in the area of the electromagnetic waves and forces in dispersive chiral particles. Methods such as Maxwell's stress tensor and Lorentz forces could be applied to compute optical forces of natural [15, 16] and artificial [14, 17] chiral media [15, 16, 17, 18, 19, 20, 21, 22, 23] based on the distributions of electromagnetic fields. However, the systematic numerical analysis of forces on core-shell nanoparticles containing dispersive and effective chiral media [22] has not been performed. It may be due to the difficulty in the treatment of the dispersive permittivity, permeability and chirality parameter, as well as magnetoelectric coupling constitutive relations.

Because there is no available analytical approach for objects of complicated shapes, some numerical approaches, such as the finite-difference time-domain (FDTD) method [11, 24, 25, 26, 27, 28], has to be employed. For the analysis of electromagnetic waves and optical forces on effective electric or magnetic dispersive particles [12], not dielectric or metal particles, the Lorentz force formula incorporated with the FDTD method for conventional nonchiral particles has been reported [11]. The wave propagation and Lorentz force density in one dimensional chiral slab is discussed [17]. The two dimensional (2D) FDTD method has the advantages of simulating chiral structures with complicated shapes illuminated by an obliquely incident plane wave. Thus, some new physical phenomena may occur.

DOI: 10.1587/elex.13.20160974
Received October 5, 2016
Accepted October 24, 2016
Publicized November 9, 2016
Copyedited November 25, 2016

In this paper, we present the Lorentz force formula for the magnetoelectric coupling and dispersive chiral media by introducing the bound charges and incorporating the auxiliary differential equations (ADE) FDTD method. With the formula, the researches on 2D composite structures composed of effective frequency-dependent dielectric, magnetic, and chiral materials become possible.

In this paper, the ADE-FDTD method is expanded to obtain the co- and cross-polarized electromagnetic field and Lorentz force density distributions in and around dispersive chiral structures. The Lorentz force density and wave equations based on the ADE-FDTD method for chiral media are theoretically derived. Very good agreement is observed by comparing the numerical results using the approaches proposed in the paper and the corresponding solutions in Ref. [11] for a dielectric cylinder illuminated by a plane wave. To discuss the trapping of chiral particles, the time-averaged Lorentz force density distributions of a single chiral cylinder, and a dielectric cylinder coated by the chiral medium contributed by bound charges and currents, are simulated. Some degrees of freedom, as well as novel functionalities can be obtained by incorporating active chiral media into microparticle sorting systems.

2 Theory

2.1 Constitutive relations and wave equations for chiral media

The constitutive relations that describe the magneto-electric coupling for the bi-isotropic medium in the frequency domain can be expressed [28, 29]

$$\begin{aligned} \boldsymbol{D}(\omega) &= \varepsilon(\omega)\boldsymbol{E} + [\chi(\omega) - \mathrm{j}\kappa(\omega)]\sqrt{\mu_0\varepsilon_0}\boldsymbol{H} \\ \boldsymbol{B}(\omega) &= \mu(\omega)\boldsymbol{H} + [\chi(\omega) + \mathrm{j}\kappa(\omega)]\sqrt{\mu_0\varepsilon_0}\boldsymbol{E} \end{aligned} \tag{1}$$

where ε, μ, χ, and κ are the frequency-dispersive permittivity, permeability, Tellegen, and chirality parameter respectively. If $\chi = 0$, it becomes a purely chiral medium.

The dispersive permittivity and permeability for chiral media generally follow Lorentzian models, and the chirality parameter follows a Condon model, that is,

$$\begin{aligned} \varepsilon(\omega) &= \varepsilon_\infty\varepsilon_0 + (\varepsilon_s - \varepsilon_\infty)\varepsilon_0\omega_e^2/(\omega_e^2 - \omega^2 + \mathrm{j}2\xi_e\omega) \\ \mu(\omega) &= \mu_\infty\mu_0 + (\mu_s - \mu_\infty)\mu_0\omega_h^2/(\omega_h^2 - \omega^2 + \mathrm{j}2\xi_h\omega) \\ \kappa(\omega) &= \tau_\kappa\omega_\kappa^2\omega/(\omega_\kappa^2 - \omega^2 + \mathrm{j}2\omega_\kappa\xi_\kappa\omega) \end{aligned} \tag{2}$$

In Eq. (2), ε_s, μ_s, ε_∞, and μ_∞ are the permittivity and permeability at zero and infinite frequencies respectively. ω_e, ω_h, and ω_κ represent resonance angular frequencies, while ξ_e, ξ_h, and ξ_κ denote damping factors. τ_κ represents a characteristic time constant measuring the magnitude of the optical activity (either chirality or gyrotropy). The medium parameters for a passive, lossy chiral medium must satisfy $\mathrm{Im}(\varepsilon) < 0$, $\mathrm{Im}(\mu) < 0$, and $\varepsilon_0\mu_0\,\mathrm{Im}^2(\kappa) < \mathrm{Im}(\mu)\,\mathrm{Im}(\varepsilon)$, otherwise the chiral medium becomes an active one [10, 30].

The relation between the electric polarization vectors $\boldsymbol{P}_e$, $\boldsymbol{P}_c$, induced electric currents $\boldsymbol{J}$, $\boldsymbol{J}_c$, and electric field $\boldsymbol{E}$, as well as the relation between the magnetic polarization vectors $\boldsymbol{M}_n$, $\boldsymbol{M}_c$, induced magnetic currents $\boldsymbol{K}$, $\boldsymbol{K}_c$, and magnetic field $\boldsymbol{H}$ can be defined as [12]

DOI: 10.1587/elex.13.20160974
Received October 5, 2016
Accepted October 24, 2016
Publicized November 9, 2016
Copyedited November 25, 2016

$$
\begin{aligned}
\boldsymbol{P}_e &= \boldsymbol{E}(\varepsilon_s - \varepsilon_\infty)\varepsilon_0\omega_e^2/(\omega_e^2 - \omega^2 + \mathrm{j}2\xi_e\omega) = \boldsymbol{J}/\mathrm{j}\omega \\
\boldsymbol{M}_n &= \boldsymbol{H}(\mu_s - \mu_\infty)\mu_0\omega_h^2/(\omega_h^2 - \omega^2 + \mathrm{j}2\xi_h\omega) = \boldsymbol{K}/\mathrm{j}\omega \\
\boldsymbol{P}_c &= \mathrm{j}\boldsymbol{E}\sqrt{\mu_0\varepsilon_0}\tau_\kappa\omega_\kappa^2\omega/(\omega_\kappa^2 - \omega^2 + \mathrm{j}2\omega_\kappa\xi_\kappa\omega) = \boldsymbol{J}_c/\mathrm{j}\omega \\
\boldsymbol{M}_c &= -\mathrm{j}\sqrt{\mu_0\varepsilon_0}\boldsymbol{H}\tau_\kappa\omega_\kappa^2\omega/(\omega_\kappa^2 - \omega^2 + j2\omega_\kappa\xi_\kappa\omega) = \boldsymbol{K}_c/\mathrm{j}\omega
\end{aligned} \tag{3}
$$

By introducing the transform relation between the frequency domain and time domain ($\mathrm{j}\omega \rightarrow \partial/\partial t$), the time-domain counterparts of Eq. (3) plus two of the Maxwell equations, namely, the electromagnetic field and current equations used to model wave propagation in chiral media are given as

$$
\begin{aligned}
&\nabla \times \boldsymbol{H} = \varepsilon_\infty\varepsilon_0\ \partial\boldsymbol{E}/\partial t + \boldsymbol{J} + \boldsymbol{K}_c \\
&\partial^2\boldsymbol{J}/\partial^2 t + 2\xi_e\ \partial\boldsymbol{J}/\partial t + \omega_e^2\boldsymbol{J} = (\varepsilon_s - \varepsilon_\infty)\varepsilon_0\omega_e^2\ \partial\boldsymbol{E}/\partial t \\
&\partial^2\boldsymbol{K}/\partial^2 t + 2\xi_h\ \partial K/\partial t + \omega_h^2\boldsymbol{K} = (\mu_s - \mu_\infty)\mu_0\omega_h^2\ \partial H/\partial t \\
&\nabla \times \boldsymbol{E} = -\mu_\infty\mu_0\ \partial H/\partial t - \boldsymbol{K} - \boldsymbol{J}_c \\
&\partial^2\boldsymbol{J}_c/\partial^2 t + 2\omega_\kappa\xi_\kappa\ \partial\boldsymbol{J}_c/\partial t + \omega_\kappa^2\boldsymbol{J}_c = \tau_\kappa\omega_\kappa^2\sqrt{\mu_0\varepsilon_0}\ \partial^2\boldsymbol{E}/\partial^2 t \\
&\partial^2\boldsymbol{K}_c/\partial^2 t + 2\omega_\kappa\xi_\kappa\ \partial\boldsymbol{K}_c/\partial t + \omega_\kappa^2\boldsymbol{K}_c = -\tau_\kappa\omega_\kappa^2\sqrt{\mu_0\varepsilon_0}\ \partial^2\boldsymbol{H}/\partial^2 t
\end{aligned} \tag{4}
$$

For two dimensional cases, the physical quantities are independent of z axis i.e. $\partial/\partial \mathrm{z} = 0$. The spatial and time iterative equations for dispersive and source-free chiral media can be developed using the ADE-FDTD method. In this paper, the transverse magnetic (TM) polarized waves are composed of E_z, H_x, H_y, and transverse electric (TE) polarized waves are composed of H_z, E_x, E_y, respectively. In Ref. [17], the 1D FDTD simulator solves the co-polarized waves for E_x and H_y, and cross-polarized waves for E_y and H_x. For simplicity, only the discretized expressions for E_z, J_{cz} and K_{cz} are given as

$$
\begin{aligned}
E_z^{n+1}(i,j) &= E_z^n(i,j) - \frac{\Delta t}{\varepsilon_\infty\varepsilon_0}\left[J_z^{n+\frac{1}{2}}(i,j) + K_{cz}^n\left(i+\frac{1}{2}, j+\frac{1}{2}\right)\right] + \frac{\Delta t}{\varepsilon_\infty\varepsilon_0} \\
&\times\left[\frac{H_y^{n+\frac{1}{2}}\left(i+\frac{1}{2}, j\right) - H_y^{n+\frac{1}{2}}\left(i-\frac{1}{2}, j\right)}{\Delta x} - \frac{H_x^{n+\frac{1}{2}}\left(i, j+\frac{1}{2}\right) - H_x^{n+\frac{1}{2}}\left(i, j-\frac{1}{2}\right)}{\Delta y}\right] \\
J_z^{n+\frac{3}{2}}(i,j) &= a_x J_z^{n+\frac{1}{2}}(i,j) + \beta_x J_z^{n-\frac{1}{2}}(i,j) + \gamma_x[E_z^{n+1}(i,j) - E_z^{n-1}(i,j)] \\
K_{cz}^{n+1}\left(i+\frac{1}{2}, j+\frac{1}{2}\right) &= a_{\kappa cx}K_{cz}^n\left(i+\frac{1}{2}, j+\frac{1}{2}\right) + \beta_{\kappa cx}K_{cz}^{n-1}\left(i+\frac{1}{2}, j+\frac{1}{2}\right) \\
&+ \gamma_{\kappa cx}\left[H_z^{n+\frac{1}{2}}\left(i+\frac{1}{2}, j+\frac{1}{2}\right) - 2H_z^{n-\frac{1}{2}}\left(i+\frac{1}{2}, j+\frac{1}{2}\right) + H_z^{n-\frac{3}{2}}\left(i+\frac{1}{2}, j+\frac{1}{2}\right)\right]
\end{aligned} \tag{5}
$$

where

$$
\begin{aligned}
&\alpha_x = \frac{2 - \omega_e^2\Delta t^2}{1 + \xi_e\Delta t}, \quad \beta_x = \frac{\xi_e\Delta t - 1}{1 + \xi_e\Delta t}, \quad \gamma_x = \frac{(\varepsilon_s - \varepsilon_\infty)\varepsilon_0\omega_e^2\Delta t/2}{1 + \xi_e\Delta t}, \\
&\alpha_{\kappa cx} = \frac{(2 - \omega_\kappa^2\Delta t^2)}{1 + \omega_\kappa\xi_\kappa\Delta t}, \quad \beta_{\kappa cx} = \frac{\omega_\kappa\xi_\kappa\Delta t - 1}{1 + \omega_\kappa\xi_\kappa\Delta t}, \quad \gamma_{\kappa cx} = -\frac{\tau_\kappa\omega_\kappa^2\sqrt{\mu_0\varepsilon_0}}{1 + \omega_\kappa\xi_\kappa\Delta t}.
\end{aligned} \tag{6}
$$

DOI: 10.1587/elex.13.20160974
Received October 5, 2016
Accepted October 24, 2016
Publicized November 9, 2016
Copyedited November 25, 2016

2.2 Lorentz force for chiral media

According to the Lorentz law [31], the Lorentz force density $F_L(r,t)$ exerted on the local charge density $\rho_{\text{total}}(r,t)$ and current density $\boldsymbol{J}_{\text{total}}(r,t)$ is

$$F_L(r,t) = \rho_{\text{total}}(r,t)\boldsymbol{E}(r,t) + \boldsymbol{J}_{\text{total}}(r,t) \times \boldsymbol{B}(r,t) \tag{7}$$

where

$$\begin{aligned} \rho_{\text{total}}(r,t) &= \rho_{\text{free}}(r,t) - \nabla \cdot \boldsymbol{P}(r,t) \\ \boldsymbol{J}_{\text{total}}(r,t) &= \boldsymbol{J}_{\text{free}}(r,t) + \partial \boldsymbol{P}(r,t)/\partial t + \mu_0^{-1} \nabla \times \boldsymbol{M} \\ \boldsymbol{E} &= (\boldsymbol{D} - \boldsymbol{P})/\varepsilon_0 \\ \boldsymbol{B} &= \mu_0 \boldsymbol{H} + \boldsymbol{M} \end{aligned} \tag{8}$$

$\rho_{\text{free}}(\boldsymbol{r},t)$ and $\boldsymbol{J}_{\text{free}}(\boldsymbol{r},t)$ are free charge and free current source densities. The bound electric charge density $\rho_{\text{e\_bound}}(\boldsymbol{r},t)$ and current density $\boldsymbol{J}_{\text{e\_bound}}(\boldsymbol{r},t)$, bound magnetic charge density $\rho_{\text{m\_bound}}(\boldsymbol{r},t)$, and current density $\boldsymbol{J}_{\text{m\_bound}}(\boldsymbol{r},t)$ can be written in terms of the electric polarization vector $\boldsymbol{P}(\boldsymbol{r},t)$, and the magnetization vector $\boldsymbol{M}(\boldsymbol{r},t)$. That is, $\boldsymbol{J}_{\text{e\_bound}}(\boldsymbol{r},t) = \partial \boldsymbol{P}(\boldsymbol{r},t)/\partial t$, $\rho_{\text{e\_bound}}(\boldsymbol{r},t) = -\nabla \cdot \boldsymbol{P}(\boldsymbol{r},t)$, $\boldsymbol{J}_{\text{m\_bound}}(\boldsymbol{r},t) = \partial \boldsymbol{M}(\boldsymbol{r},t)/\partial t$, and $\rho_{\text{m\_bound}}(\boldsymbol{r},t) - \nabla \cdot \boldsymbol{M}(\boldsymbol{r},t)$.

The generalized expression of the Lorentz force density exerted by the electromagnetic fields on normal media is [31]

$$\begin{aligned} \boldsymbol{F}_1(\boldsymbol{r},t) = \rho_{\text{free}}\boldsymbol{E} + \boldsymbol{J}_{\text{free}} \times \mu_0 \boldsymbol{H} + (\boldsymbol{P} \cdot \nabla)\boldsymbol{E} + (\boldsymbol{M} \cdot \nabla)\boldsymbol{H} \\ + \frac{\partial \boldsymbol{P}}{\partial t} \times \mu_0 \boldsymbol{H} - \frac{\partial \boldsymbol{M}}{\partial t} \times \varepsilon_0 \boldsymbol{E} \end{aligned} \tag{9}$$

The alternative and equivalent formula for the Lorentz force density is

$$\begin{aligned} \boldsymbol{F}_2(\boldsymbol{r},t) = (\rho_{\text{free}} - \nabla \cdot \boldsymbol{P})\boldsymbol{E} + \left(\boldsymbol{J}_{\text{free}} + \frac{\partial \boldsymbol{P}}{\partial t}\right) \times \mu_0 \boldsymbol{H} \\ - (\nabla \cdot \boldsymbol{M})\boldsymbol{H} - \frac{\partial \boldsymbol{M}}{\partial t} \times \varepsilon_0 \boldsymbol{E} \end{aligned} \tag{10}$$

The magnetic induction B for dispersive chiral media can be rewritten as

$$\boldsymbol{B} = \mu_0 \boldsymbol{H} + \boldsymbol{M} = \mu_\infty \mu_0 \boldsymbol{H} + (\boldsymbol{M}_n + \boldsymbol{P}_c) \tag{11}$$

Substituting Eq. (11) into two of the Maxwell equations, one can arrive at

$$\nabla \cdot \boldsymbol{B} = \nabla \cdot (\mu_0 \boldsymbol{H} + \boldsymbol{M}) = 0 \tag{12}$$

$$\begin{aligned} \nabla \times \boldsymbol{E} &= -\partial \boldsymbol{B}/\partial t = -\mu_0 \partial \boldsymbol{H}/\partial t + \partial \boldsymbol{M}/\partial t \\ &= -\mu_0 \mu_\infty \partial \boldsymbol{H}/\partial t - \partial(\boldsymbol{M}_n + \boldsymbol{P}_c)/\partial t \end{aligned} \tag{13}$$

The bound magnetic charge density is defined as

$$\rho_{\text{m\_bound}} = \mu_0 \nabla \cdot \boldsymbol{H} = -\nabla \cdot \boldsymbol{M} \tag{14}$$

Eq. (13) can be rearranged as follows

$$-\mu_0 \frac{\partial \boldsymbol{H}}{\partial t} = \frac{\nabla \times \boldsymbol{E} + \partial(\boldsymbol{M}_n + \boldsymbol{P}_c)/\partial t}{\mu_\infty} \tag{15}$$

$$\begin{aligned} \boldsymbol{J}_{\text{m\_bound}} = \frac{\partial \boldsymbol{M}}{\partial t} = -\mu_0 \frac{\partial \boldsymbol{H}}{\partial t} - \nabla \times \boldsymbol{E} = \frac{\nabla \times \boldsymbol{E} + \partial(\boldsymbol{M}_n + \boldsymbol{P}_c)/\partial t}{\mu_\infty} - \nabla \times \boldsymbol{E} \\ = \frac{\partial(\boldsymbol{M}_n + \boldsymbol{P}_c)/\partial t}{\mu_\infty} + \frac{(1 - \mu_\infty)\nabla \times \boldsymbol{E}}{\mu_\infty} \end{aligned} \tag{16}$$

DOI: 10.1587/elex.13.20160974
Received October 5, 2016
Accepted October 24, 2016
Publicized November 9, 2016
Copyedited November 25, 2016

In Eq. (16), the bound magnetic current density is determined by the magnetic polarization vector $\boldsymbol{M}_n$ and the coupled electric polarization vector P_c.
In a similar derivation process, the corresponding expression formulas for the bound electric charge density $\rho_{\text{e\_bound}}$ and bound electric current density $\boldsymbol{J}_{\text{e\_bound}}$ can be got

$$\begin{aligned}\rho_{\text{e\_bound}} &= \varepsilon_0 \nabla \cdot \boldsymbol{E} = -\nabla \cdot \boldsymbol{P} \\ \boldsymbol{J}_{\text{e\_bound}} &= [\partial(\boldsymbol{P}_e + \boldsymbol{M}_c)/\partial t + (\varepsilon_\infty - 1)(\nabla \times \boldsymbol{H})]/\varepsilon_\infty\end{aligned} \tag{17}$$

The electromagnetic fields, charges, and currents are functions of the time and spatial coordinates. Thus, the force density distribution can be computed by time-averaging the Lorentz force density,

$$\begin{aligned}\langle \boldsymbol{F} \rangle = &\frac{1}{T}\int_0^T (\rho_{\text{free}}\boldsymbol{E} + \rho_{\text{e\_bound}}\boldsymbol{E} - \boldsymbol{J}_{\text{m\_bound}} \times \varepsilon_0 \boldsymbol{E})dt \\ &+ \frac{1}{T}\int_0^T (\boldsymbol{J}_{\text{free}} \times \mu_0 \boldsymbol{H} + \boldsymbol{J}_{\text{e\_bound}} \times \mu_0 \boldsymbol{H} + \rho_{\text{m\_bound}}\boldsymbol{H})dt\end{aligned} \tag{18}$$

the time integral in Eq. (18) can be taken over in one period of 2D time-harmonic fields.

By substituting Eqs. (14), (16), and (17) into Eq. (18), the x and y components of the Lorentz force densities for TM polarized waves contributed by bound charge and current densities in sourceless chiral media are

$$\begin{aligned}F^x_{\text{TMcharge}} &= \mu_0 H_x(\partial H_x/\partial x + \partial H_y/\partial y) \\ F^y_{\text{TMcharge}} &= \mu_0 H_y(\partial H_x/\partial x + \partial H_y/\partial y) \\ F^x_{\text{TMcurrent}} &= \begin{bmatrix} \mu_0(\varepsilon_\infty - 1)\left(\dfrac{\partial H_x}{\partial y}H_y - \dfrac{\partial H_y}{\partial x}H_y\right) \Big/ \varepsilon_\infty - \dfrac{\mu_0(J_z + K_{cz})H_y}{\varepsilon_\infty} \\ -\dfrac{\varepsilon_0(K_y + J_{cy})E_z}{\mu_\infty} + \varepsilon_0(1 - \mu_\infty)\dfrac{\partial E_z}{\partial x}E_z/\mu_\infty \end{bmatrix} \\ F^y_{\text{TMcurrent}} &= \begin{bmatrix} \mu_0(\varepsilon_\infty - 1)\left(\dfrac{\partial H_y}{\partial x}H_x - \dfrac{\partial H_x}{\partial y}H_x\right) \Big/ \varepsilon_\infty + \dfrac{\mu_0(J_z + K_{cz})H_x}{\varepsilon_\infty} \\ +\dfrac{\varepsilon_0(K_x + J_{cx})E_z}{\mu_\infty} + \varepsilon_0(1 - \mu_\infty)\dfrac{\partial E_z}{\partial y}E_z/\mu_\infty \end{bmatrix}\end{aligned} \tag{19}$$

However, the z component of the Lorentz force density for TM polarized waves cannot be separated individually. The force density in the z-direction for the infinite chiral cylinder can only be decomposed into components contributed by bound charges and currents as

$$\begin{aligned}F^z_{\text{charge}} &= \varepsilon_0 E_z(\partial E_x/\partial x + \partial E_y/\partial y) + \mu_0 H_z(\partial H_x/\partial x + \partial H_y/\partial y) \\ &= P_x \partial E_z/\partial x + P_y \partial E_z/\partial y + M_x \partial H_z/\partial x + M_y \partial H_z/\partial y\end{aligned} \tag{20}$$

$$F^z_{\text{current}} = \begin{bmatrix} \dfrac{\mu_0(J_{px}H_y - J_{py}H_x)}{\varepsilon_\infty} + \mu_0(\varepsilon_\infty - 1)\left(\dfrac{\partial H_z}{\partial y}H_y + \dfrac{\partial H_z}{\partial x}H_x\right) \Big/ \varepsilon_\infty \\ -\dfrac{\varepsilon_0(J_{mpx}E_y - J_{mpy}E_x)}{\mu_\infty} - \varepsilon_0(1 - \mu_\infty)\left(\dfrac{\partial E_z}{\partial y}E_y + \dfrac{\partial E_z}{\partial x}E_x\right) \Big/ \mu_\infty \end{bmatrix}$$

DOI: 10.1587/elex.13.20160974
Received October 5, 2016
Accepted October 24, 2016
Publicized November 9, 2016
Copyedited November 25, 2016

By using a Yee cell and incorporating the FDTD method, one can further obtain the discretized components of the Lorentz force density. Instead of the average electric and magnetic fields, the spatial averaging medium parameters [24, 28] such as ε_s, ε_∞, ω_e, ξ_e in Eq. (2) are applied to the iterative equations at the media boundaries in this paper. Thus numerical artifacts and discontinuities of the Maxwell and Lorentz force equations can be eliminated.

3 2D FDTD simulations

In the following section, first, we provide the verification of approaches and programs for the ADE-FDTD method. Then, we study the co-polarized, cross-polarized, and net Lorentz force densities exerted on single cylindrical rod and a coated cylinder containing chiral medium, respectively. The mechanical interaction between a plane wave and chiral structures is numerically investigated.

3.1 Lorentz force for chiral media

The Lorentz force intensities for a Gaussian beam in a dielectric cylinder with $\varepsilon_r = 4$ and radius $r = 40\delta$ are illustrated in Fig. 1. The cylinder is located at $(x, y) = (111\delta, 147\delta)$. The TM polarized beam $\mathrm{E_{in}} = 10^3 \exp[-(x/x_0)^2] \sin(\omega_0 t)$ V/m at $y = 50\delta$ is incident from up to bottom along the $+y$-direction. The amplitude of the full width at half maximum (FWHM) is 0.5 μm and the value of x_0 is 0.3 μm. The FDTD cell sizes are $\Delta x = \Delta y = \delta = \lambda_0/130 = 5$ nm. The relative permittivity of the cylinder linearly changes from 4 to 1 at the surface, that is, in a 4δ-thickness transition layer. The integrated forces is $\int f_x(x, y)\mathrm{d}x\mathrm{d}y = -0.14$ pN/m contributed by the bound electric current density $\boldsymbol{J}_{\mathrm{e\_bound}}(\boldsymbol{r}, \mathrm{t})$. The force densities in this paper are calculated by time-averaging the Lorentz equation from $t = 1135\Delta t$ in one period of the time harmonic electromagnetic fields. It should be noted that the numerical results may slightly change if the period of the time harmonic electromagnetic fields is different. The numerical results are in good agreement with the solutions of the s-light in Ref. [11] to verify the accuracy of the FDTD approach and Lorentz force density approach in this paper to some extent.

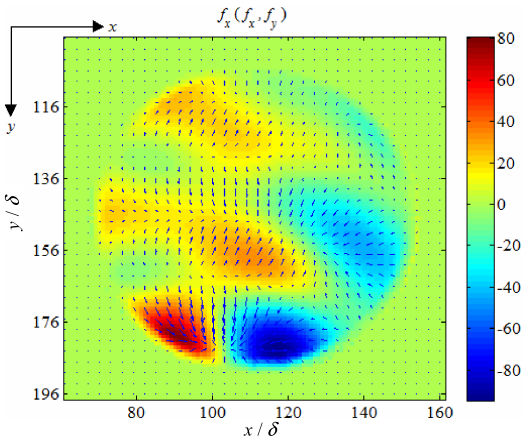

Fig. 1. Distribution of force intensities $f_x(f_x, f_y)$ for a dielectric cylinder illuminated by a TM polarized Gaussian beam.

DOI: 10.1587/elex.13.20160974
Received October 5, 2016
Accepted October 24, 2016
Publicized November 9, 2016
Copyedited November 25, 2016

3.2 Force densities exerted by a plane wave on a chiral cylinder rod

In Fig. 2 and Fig. 3, the initial E-field and H-field amplitudes of the incident TM waves are $E_0 = 10^3\,\mathrm{V/m}$ and $H_0 = 2.6544\,\mathrm{A/m}$, respectively. The integrated Poynting vector (per unit length along the y axis of the incident plane wave) is $\int S_y(x, y)\mathrm{d}x = \int 0.5E_0H_0\mathrm{d}x = 2\,\mathrm{mW/m}$. The FDTD grid cell size is $\delta = 5\,\mathrm{nm}$ and time-step size is $\Delta t = \delta/2c$. There are 301×296 Yee cells in the whole simulation region reported below. Fig. 2 illustrates the interaction between a continuous plane wave and a dispersive chiral cylinder. The working frequency of interest is assumed to be $f_0 = 468.75\,\mathrm{THz}$. The continuous plane wave is at $y = 50\delta$ and propagates in free-space along the positive y-direction. In Fig. 2, the medium parameters for the chiral cylinder are $\varepsilon_s = 1.08\varepsilon_0$, $\varepsilon_\infty = \varepsilon_0$, $\mu_s = 1.1\mu_0$, $\mu_\infty = \mu_0$, $\omega_e = 2\pi \times 260\,\mathrm{THz}$, $\omega_h = 2\pi \times 240\,\mathrm{THz}$, $\omega_k = 2\pi \times 100\,\mathrm{THz}$, $\xi_e = 1200\omega_e$, $\xi_h = 1400\omega_h$, $\xi_k = 2.5$, and $\tau_k = 4.8 \times 10^{-17}\,\mathrm{s}$. That is, ε_r, μ_r, and κ_r at f_0 are $1 - \mathrm{j}1.85 \times 10^{-5}$, $1 - \mathrm{j}1.83 \times 10^{-5}$, and $-0.003 - \mathrm{j}0.003$, respectively. The radius of the cylinder is 200 nm. The chiral media discussed in this paper are active due to their $\varepsilon_0\mu_0\,\mathrm{Im}(\kappa)^2 > \mathrm{Im}(\varepsilon)\,\mathrm{Im}(\mu)$. The gain property is caused by the chirality parameter instead of the permittivity or permeability with a positive imaginary part.

The $|E_z|$ component of the co-polarized TM light and $|H_z|$ component of the coupled cross-polarized TE light measured at time $t = 1135\Delta t$ are shown in Fig. 2(a) and 2(b), respectively. If the chirality parameter is deducted, the chiral cylinder shown in Fig. 2 nearly becomes an impedance matched medium to the free space. Thus, the co-polarized reflective electric field is very small and the $|E_z|$ seems to be hardly influenced by the chiral cylinder. In Fig. 2(b), the coupled $|H_z|$ engendered by the cylinder resembles a small point source in the cylinder. Meanwhile, the chiral cylinder functions as a convex lens, which make the cross-polarized waves form a focus at the edge of the cylinder. The focused light beam produced by the cross-polarized waves can capture the cylinder as the gradient force overcomes the scattering force due to the inhomogeneous field intensities.

In Fig. 2(c)–(f), the co-polarized and cross-polarized time-averaged force density distributions are shown with the corresponding (f_x, f_y) vector fields superposed. Fig. 2(c) and (e) give the co-polarized force densities f_x and f_y contributed by the bound current and charge densities, respectively. In Fig. 2(c) and (e), the time-averaged pushing force densities in the chiral cylinder near the TM incident source are relatively larger than those away from the source. However, the time-averaged pulling force densities generated by bound electric and magnetic current densities are much larger where the cross-polarized TE light departs from the cylinder in Fig. 2(d) and (f). As the cross-polarized TE waves are continuously coupled out from the co-polarized TM waves, the absolute values of the force densities contributed by bound currents for TE light increase and contributed by bound currents for TM light decrease along the positive y axis. The distribution of force densities generated by the bound electric and magnetic charges is inhomogeneous at the surface of the chiral cylinder.

The integrated force density along y-direction for co-polarized TM light is $\int f_y(x, y)\mathrm{d}x\mathrm{d}y = 1.0 \times 10^{-4}\,\mathrm{PN/m}$, and for cross-polarized TE light is $-3.1 \times 10^{-4}\,\mathrm{PN/m}$ without the surface-charge contribution. The integrated force density exerted by the bound charges are $\int f_y(x, y)\mathrm{d}x\mathrm{d}y = 1.7 \times 10^{-8}\,\mathrm{PN/m}$ and $4.7 \times$

DOI: 10.1587/elex.13.20160974
Received October 5, 2016
Accepted October 24, 2016
Publicized November 9, 2016
Copyedited November 25, 2016

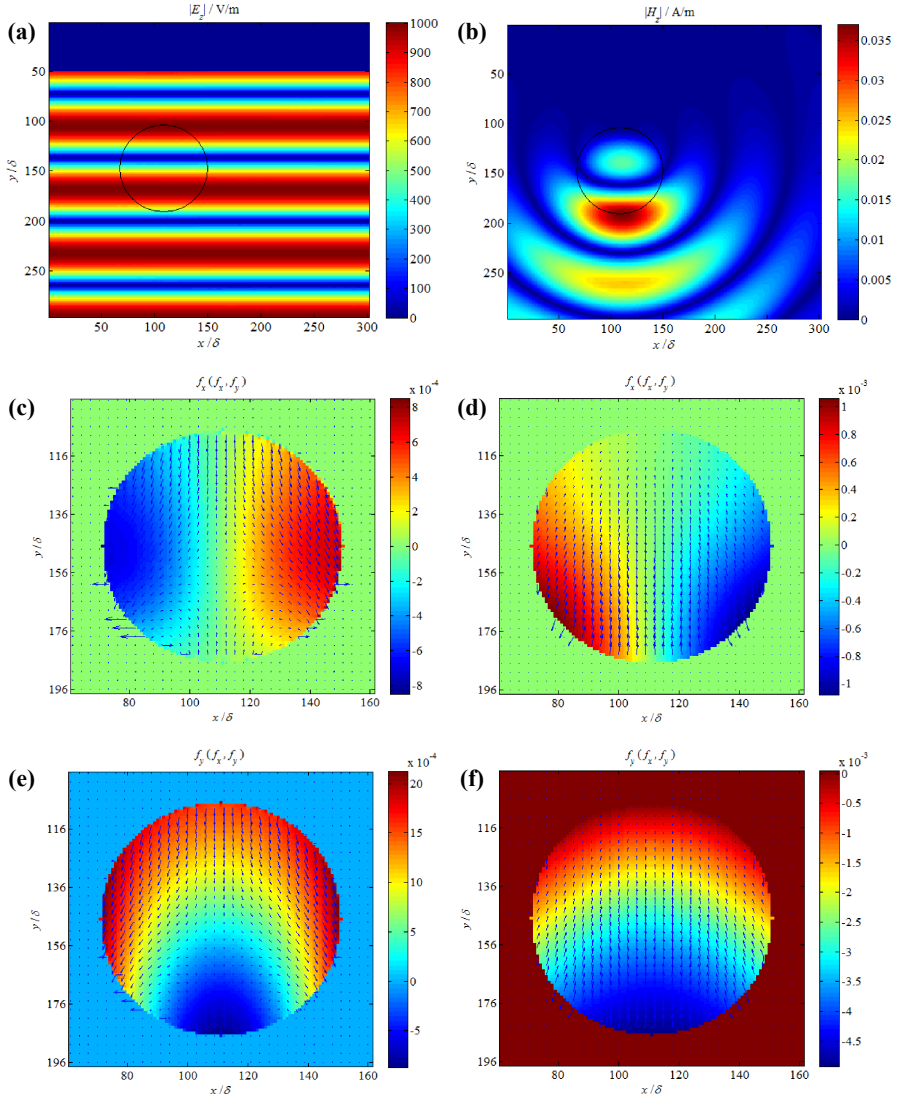

Fig. 2. FDTD computed electromagnetic waves and force densities of a chiral cylinder rod centered at $(x, y) = (111\delta, 147\delta)$. (a) Time snapshot of $|E_z|$ distribution for TM light, (b) Time snapshot of $|H_z|$ for TE light, (c) Distribution of f_x for TM light, (d) Distribution of f_x for TE light, (e) Distribution of f_y for TM light, (f) Distribution of f_y for TE light.

10^{-5} PN/m for TM and TE light, respectively. The net integrated force density is -1.6×10^{-4} PN/m along the y-direction. One can conclude that the bound current density, induced by the active chirality parameter, for the TE light plays an important role in pulling the cylinder backward. The optical rotation can be characterized by the co- and cross-polarized light. Thus, the optical pulling force density on the chiral cylinder can be explained by the large optical rotation, which is possessed by active chiral media and induces the rotation of the plane of the incident polarized light.

3.3 A dielectric cylinder coated by a chiral medium illuminated by a plane wave

Fig. 3 displays the co- and cross-polarized Lorentz force densities of a dielectric cylinder (radius $r = 40$ nm, relative permittivity and permeability $\varepsilon_r = \mu_r = 1.02$)

DOI: 10.1587/elex.13.20160974
Received October 5, 2016
Accepted October 24, 2016
Publicized November 9, 2016
Copyedited November 25, 2016

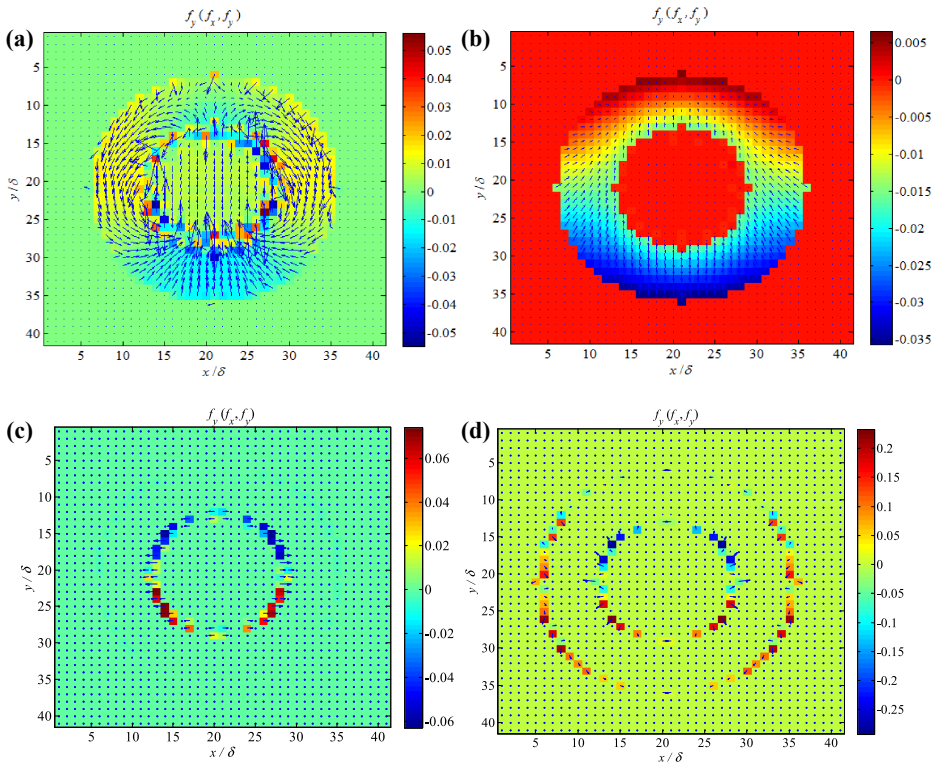

Fig. 3. Co- and cross-polarized time-averaged force densities of a dielectric cylinder ($\varepsilon_r = \mu_r = 1.02$) coated by a chiral medium. (a) contributed by bound currents for TM light, (b) contributed by bound currents for TE light, (c) contributed by bound charges for TM light, (d) contributed by bound charges for TE light.

covered by a 35 nm-thickness chiral medium. The center frequency of the incident plane wave is chosen to be $f_0 = 461.54$ THz. The medium parameters for the chiral medium in Eq. (2) are $\varepsilon_s = 1.1\varepsilon_0$, $\varepsilon_\infty = \varepsilon_0$, $\mu_s = 1.1\mu_0$, $\mu_\infty = \mu_0$, $\omega_e = \omega_h = 2\pi \times 250$ THz, $\omega_k = 2\pi \times 100$ THz, $\xi_e = 1500\omega_e$, $\xi_h = 1500\omega_h$, $\xi_k = 3$, $\tau_k = 3.5 \times 10^{-16}$ s, i.e. ε_r, μ_r, and κ_r at f_0 are approximately $1 - \mathrm{j}1.78 \times 10^{-5}$, $1 - \mathrm{j}1.78 \times 10^{-5}$ and $-0.018 - \mathrm{j}0.024$.

In Fig. 3(a), the co-polarized time-averaged force densities contributed by bound currents are much larger at the media boundaries between dielectric and chiral medium. The force densities near the y axis seem to pull the coated cylinder toward the incident source, whereas the force densities apart from the y axis seem to push the coated cylinder. In Fig. 3(b), the cross-polarized time-averaged force densities in the dielectric layer contributed by bound currents for the coupled TE light are zero, because there are no induced bound currents in the dielectric layer. Meanwhile, the cross-polarized waves coupled by the coated chiral layer have no impact on the inner dielectric cylinder.

As can be seen in Fig. 3(c), the time-averaged force densities engendered by bound electric and magnetic charges for the TM light at the discontinuous media boundary between the dielectric and chiral medium are so big that the interfacial force densities at the media boundary between the chiral medium and free space can hardly be seen. However, the distribution of the Lorentz force density for the TE light is relative homogeneous on the two media boundaries in Fig. 3(d). The

DOI: 10.1587/elex.13.20160974
Received October 5, 2016
Accepted October 24, 2016
Publicized November 9, 2016
Copyedited November 25, 2016

net integrated force density of the coated cylinder is $\int f_y(x, y)\mathrm{d}x\mathrm{d}y = -2.5 \times 10^{-5}$ PN/m along the y-direction. We notice that the introduction of the chiral layer on the surface of the dielectric cylinder tends to make the coated cylinder pull backward in the y-direction. The vertical trapping mainly benefits from the cross-polarized waves contributed by the bound electric and magnetic currents, which are induced by the chirality parameter.

4 Conclusion

The wave propagation and optical pulling Lorentz force density within the dispersive chiral cylinder are studied using the ADE-FDTD method in this paper. By introducing the coupled electric and magnetic polarization vectors, we deduce the time–averaged Lorentz force density for the dispersive and magneto–electric coupling chiral media based on the electromagnetic fields, bound electric and magnetic charge densities, as well as bound electric and magnetic current densities. We find that the gradient force overcomes the scattering force as the cross-polarized magnetic field in active chiral cylinder is coupled out and acts like a point source. Numerical results show that the capture of the dielectric cylinder coated by the active chiral medium is mainly contributed by the cross-polarized bound currents in the chiral medium. However, their contribution to the Lorentz force density in the inner dielectric layer is zero. The reported finding may provide some guidelines for the light-chiral media mechanical coupling and propose a way of the material engineering to realize the optical trapping.

Acknowledgments

This work is supported by the Fundamental Research Funds for the Central Universities (ZYGX2015J041, ZYGX2015J039), the National Natural Science Foundation of China (41304119, 41104097, 11504252) and the Specialized Research Fund for the Doctoral Program of Higher Education (20120185120012).

DOI: 10.1587/elex.13.20160974
Received October 5, 2016
Accepted October 24, 2016
Publicized November 9, 2016
Copyedited November 25, 2016